2020 IEEE International Conference on Robotics and Automation (ICRA)
31 May - 31 August, 2020. Paris, France

Generating Visibility-Aware Trajectories for Cooperative and Proactive Motion Planning

Noam Buckman[1], Alyssa Pierson[1], Sertac Karaman[2], and Daniela Rus[1]

***Abstract*— The safety of an autonomous vehicle not only depends on its own perception of the world around it, but also on the perception and recognition from other vehicles. If an ego vehicle considers the uncertainty other vehicles have about itself, then by reducing the estimated uncertainty it can increase its safety. In this paper, we focus on how an ego vehicle plans its trajectories through the blind spots of other vehicles. We create visibility-aware planning, where the ego vehicle chooses its trajectories such that it reduces the perceived uncertainty other vehicles may have about the state of the ego vehicle. We present simulations of traffic and highway environments, where an ego vehicle must pass another vehicle, make a lane change, or traverse a partially-occluded intersection. Emergent behavior shows that when using visibility-aware planning, the ego vehicle spends less time in a blind spot, and may slow down before entering the blind spot so as to increase the likelihood other vehicles perceive the ego vehicle.**

I. Introduction

Autonomous vehicles provide a promise of safer driving on roads. Recent research has focused on developing control and perception systems that ensure safe behaviors for autonomous vehicles. This includes collision-free trajectory generation, interacting with human drivers on the road, and intent recognition of other drivers. However, a major challenge remains in ensuring safe drivers around other human drivers. Autonomous vehicles must not only react to the behaviors of surrounding vehicles, but also proactively plan to encourage safe behaviors. When driving around human drivers, it is imperative to consider their blind spots and improve mutual safety. In this paper, we consider the problem of generating trajectories that improve the visibility of the ego vehicle among neighboring vehicles. Blind spots are one example where visibility of the ego vehicle is reduced, and the particular case we focus on in this paper. Other examples of reduced visibility include driving at night, occlusions from heavy fog or other weather, or sensor failures of other vehicles. If an ego vehicle remains in a blind spot of another vehicle for too long, this decreases the safety of both vehicles and may lead to a dangerous situation, like attempting to merge into an occupied lane. If the ego vehicle can proactively adjust its trajectory to minimize this time in blind spots, it can increase its safety.

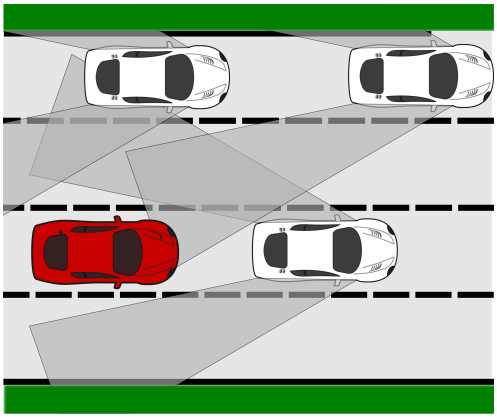

Fig. 1: For the ego vehicle (red), our approach considers the uncertainty of other drivers when planning trajectories. Specifically, we consider "visibility-aware" trajectories for an ego vehicle traversing through blind spots, such that in reduces the uncertainty other vehicles have about the ego vehicle.

Our approach is to explicitly model the perception of neighboring vehicles and use the uncertainty in their estimates to score the trajectories of the ego vehicles. We generate the model of uncertainty for other vehicles from the geometry of their blind spots, and assume that other vehicles keep a temporal history of the ego vehicle's position. Thus, if an ego vehicle is visible prior to entering the blind spot, it does not instantaneously disappear to the other vehicle, rather, the uncertainty increases until the ego vehicle becomes visible again. The ego vehicle modifies a baseline trajectory to improve the estimates of other vehicles about its position, increasing the safety of all vehicles. We utilize an optimization approach which directly minimizes the variance of the estimate, allowing the autonomous vehicle to choose trajectories that balance its own comfort with increased visibility.

A. Case Studies

We consider the following traffic scenarios to study. Each of these scenarios demonstrates a situation where an ego vehicle is occluded from a surrounding vehicle, posing a potential risk of collision.

1) Lane Changing with Blind Spots: We consider a two-lane driving environment, where vehicles must perform overtaking maneuvers. Here, we study how an ego vehicle can

[1]CSAIL, Massachusetts Institute of Technology, Cambridge, MA [nbuckman, apierson, rus] at mit.edu
[2]LIDS, Massachusetts Institute of Technology, Cambridge, MA 02139, USA sertac at mit.edu

The authors would like to thank Wilko Schwarting for his insight on belief-space planning and trajectory optimization.
This work was supported by a National Defense Science & Engineering Graduate Fellowship, NSF Grant 1723943, the Office of Naval Research (ONR) Grant N00014-18-1-2830, and Toyota Research Institute (TRI). This article solely reflects the opinions and conclusions of its authors and not TRI or any other Toyota entity. Their support is gratefully acknowledged.

maneuver through the blind spots of other vehicles while changing lanes. Visibility-aware trajectories minimize the time in blinds spots and ensure the leading vehicle has opportunities to reduce its uncertainty in its estimate of the ego vehicle.

2) Case 2: Visual Obstructions at Intersections: In busy intersections, cross traffic vehicles may have difficulty observing an ego vehicle due to visual obstructions (trees, traffic signs, buildings, other vehicles). Without an accurate estimate of the ego vehicle's position, a cross-traffic vehicle may need to brake abruptly once it see the ego vehicle or in the worst case, dangerously cross traffic at the same time as the ego vehicle.

3) Case 3: Braking Into Blind Spot: We consider how a vehicle plans a stopping maneuver when the desired final location is within the blind spot of another vehicle. A visibility-aware ego vehicle can modify its actions as it approaches a blind spot to reduce the uncertainty of surrounding vehicles, such as reducing its speed as it enters a blind spot. In turn, neighboring vehicles will become more confident about the ego vehicle's, even if their view is completely obstructed.

B. Related Work

Much research has explored safe planners that consider the risk and uncertainty of autonomous vehicles [1], [2], [3], [4], [5]. In an effort to increase safety, prior work considers how to design controllers that can interact with human pedestrians and traffic [6], [7], [8] as well as methods for interacting cooperatively with other robots [9], [10], [11], [12], [13]. More recently, [14] incorporated the responses of surrounding vehicles to generate game-theoretic trajectories. In [15], the authors model the perception of human drivers and use it to generate trajectories that communicate a vehicle intent. In both, the trajectories are optimized using the internal reward structure of the vehicles, whereas we focus on the uncertainty of the vehicle's position. If robots are fully cooperative, information gathering can be achieved by optimizing over the entire team's mutual information [16] or maintaining team observability [17]. However, unlike in team settings, vehicles on the road act as independent, rational agents who optimize their own cost function rather than a team-wide cost. Furthermore, around human drivers, we cannot rely on being able to directly communicate with those other drivers.

Belief-space planning combines the estimation dynamics with robot control to account for motion and sensing uncertainty in partially-observable Markov decision process. In [18], [19] an Extended Kalman Filter (EKF) is used estimate the robot's own state and incorporate it with a linear quadratic regulator controller to optimally control the robot. Similarly, [20] presents a rapidly-exploring random tree approach where the robot's belief is propagated through the tree and used to generate collision-free motions for the robot. To integrate visibility in the planning, [21] and [22] address planning for occluded intersections and turns, specifically considering the decision and risk of entering an intersection rather than improving visibility of the ego vehicle. Ref. [23] considers visibility optimization by using a geometric argument for maximizing visibility and directly maximize the ego vehicle's field-of-view using the geometry of the relative car positions. Our approach optimizes the estimate covariance directly, which accounts for both the perception model of the other vehicles and the accumulation of visibility throughout the trajectory.

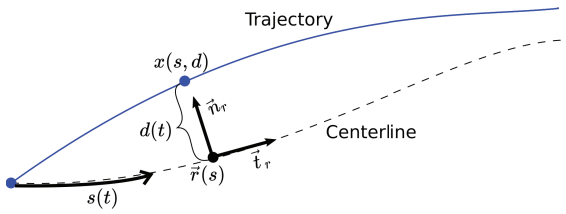

Fig. 2: Frenet Frame

In summary, the main contributions of this paper are:

- A trajectory generator that improves an autonomous vehicle's visibility by minimizing the estimate uncertainty of surrounding vehicles,
- Covariance-based costs and perception model to quantify a trajectory's visibility, and
- Simulations of our method in lane change, intersection, and braking traffic scenarios.

The remainder of the paper is organized as follows: in Section II, we present our problem definition and baseline trajectory optimization. Section III introduces our visibility-aware optimization and perception models. Analysis of simulation results is presented in Section IV, and we present our conclusions in Section V.

II. Trajectory Generation

Consider a vehicle with position $\boldsymbol{x}_t \in \mathbb{R}^2$. Our goal is to generate a trajectory of points $\boldsymbol{\xi} = \{\boldsymbol{x}_1, \boldsymbol{x}_2, \ldots, \boldsymbol{x}_T\}$ for an autonomous ego vehicle v_i as it executes a traffic maneuver. A higher-level planner provides a set of waypoints $\boldsymbol{w}_1, \ldots \boldsymbol{w}_n$ that execute the traffic maneuver such as a lane change, overtaking, or braking. Our goal is to generate a trajectory that is both dynamically feasible (considering maximum velocity, acceleration and curvature) and collision-free with other vehicle trajectories while minimizing a given cost function. Other vehicles exist on the road with the ego vehicle, executing their own trajectories $\boldsymbol{\xi}_j$ and maintain collision-free motions. Unless otherwise noted, we consider a single vehicle v_j that leads the ego vehicle.

A. Quintic Spline Trajectory Optimization

Following [24], we employ a *Frenet Frame* method for optimizing over lateral and longitudinal deviations from a given centerline trajectory. A centerline $\boldsymbol{\xi}_c$ is first computed from the waypoints, beginning at the vehicle's current position $\boldsymbol{p}_0$ and ending at the terminal point on the centerline, $\boldsymbol{p}_f$, and parameterized by arc length $s(t)$. The lateral deviations are parameterized by a distance $d(t)$ in the $\boldsymbol{n}_r$ normal direction and longitudinal deviations in the $\boldsymbol{t}_r$ direction such that trajectory from the root point $\boldsymbol{r}$ is

$$\boldsymbol{x}(s(t), d(t)) = \boldsymbol{r}(s(t)) + d(t)\boldsymbol{n}_r(s(t)). \tag{1}$$

Figure 2 shows the Frenet Frame that is used for generating and scoring trajectories. Quintic splines are generated for both dimensions and are each uniquely specified by the initial position $P_0 = [p_0, \dot{p}_0, \ddot{p}_0]$ and terminal position $P_f = [p_f, \dot{p}_f, \ddot{p}_f]$ over the duration of time $T = t_f - t_0$. Thus by varying the terminal conditions, allowing for lateral and longitudinal deviations, and duration of the maneuver T, we can generate multiple candidate trajectories. Each candidate trajectory is checked for constraints and collisions.

An advantage of using quintic candidate splines is that it has been to shown [25] to optimally minimize the squared jerk of the trajectory $J_T(p(t))$, where

$$J_T(p(t)) = \int_{t_0}^{t_0+T} \dddot{p}^2(\tau) d\tau. \tag{2}$$

Minimizing the squared jerk is a common proxy for driver comfort. An overall baseline trajectory cost is formed by adding costs on the terminal state $p_f, \dot{p}_f$ and duration of the maneuver T. We focus on lateral tracking, which utilizes a baseline cost

$$C_d(\boldsymbol{\xi}) = k_J J_T(d) + k_T T + k_p d_f^2, \tag{3}$$

where the lateral displacement at d_f at the final point is penalized. Similarly, the longitudinal cost can be formulated to encourage the ego vehicle to maintain terminal conditions with the following longitudinal cost

$$C_s(\boldsymbol{\xi}) = k_J J_T(s) + k_T T + k_{\dot{s}}[\dot{s}_f - \dot{s}_f^*]^2 + k_s[s_f - s_f^*]^2, \tag{4}$$

with desired final position s_f^* and final speed $\dot{s}_f^*$. The final baseline cost is a linear combination of each spline cost

$$C_{baseline}(\boldsymbol{\xi}) = k_{lat} C_d(\boldsymbol{\xi}) + k_{lon} C_s(\boldsymbol{\xi}). \tag{5}$$

A set of candidate trajectories is computed by varying terminal conditions for the quintic splines and then the baseline score is computed for each trajectory. Finally, the minimum cost trajectory is chosen and executed by the vehicle.

B. Perception & Prediction Model

A key insight of this work is that the ego vehicle should consider the perception of the vehicles surrounding it. We assume that all the vehicles on the road make a prediction of the ego vehicle's position $\hat{\boldsymbol{x}}_i^j$ based on local measurements $\boldsymbol{y}_t^j$ such that

$$\hat{\boldsymbol{x}}_{i,t}^j = h(\boldsymbol{y}_t^j, \hat{\boldsymbol{x}}_{i,1}^j, \ldots, \hat{\boldsymbol{x}}_{i,t-1}^j). \tag{6}$$

Importantly, the ego vehicle will consider $\hat{\boldsymbol{x}}_{i,t}^j$ in generating its own trajectories by ensuring that v_j's uncertainty is minimized throughout the trajectory. In addition, if the perception model is known, the ego vehicle can compute the covariance of the estimate $\mathbb{E}[\hat{\boldsymbol{x}}_i^{j2}]$ and use it as an optimization metric to minimize v_j's uncertainty

$$\min g(\mathbb{E}[\hat{\boldsymbol{x}}_{i,t}^{j2}]), \tag{7}$$

which will be combined with baseline cost (5).

We consider two perception models that may be maintained by the leading vehicles. In the first scenario, the ego vehicle's dynamics are known to v_j and an Extended Kalman Filter (EKF) is used to update the estimate, where the measurement noise is depends on the ego vehicle being visible to the leading vehicle. In the second scenario, we relax the dynamics assumption and assume purely limits on the control inputs of the ego vehicle.

In both perception models, the ego vehicle must maintain a prediction of the other vehicle's motion. Specifically, vehicle i can predict the future positions of the v_j: $\hat{\boldsymbol{\xi}}_j = \{\boldsymbol{x}_{j,1}, \ldots \boldsymbol{x}_{j,T}\}$ over some planning horizon T. These future positions can then be used to predict blinds spots and sensor limits when considering the perception of v_j. While predicting other vehicle's positions may not always be possible, we consider this a reasonable assumption for the purpose of collision-avoidance and perception.

III. Visibility Optimization

In this section, we describe the visibility optimization which selects trajectories that minimize the estimate uncertainty of surrounding vehicles, summarized in Algorithm 1 and illustrated in Fig. 3.

Algorithm 1 Visibility-Aware Trajectory Generation

```
Initialize mincost = ∞, ξ_min = ∅
for T ∈ T_sample, d_f ∈ d_sample, ṡ_f ∈ s_sample do
    d(t), s(t) ← Generate quintic splines(T, d_f, ṡ_f)
    ξ ← Convert splines to global coord(ξ_c, d(t), s(t))
    if ξ feasible and collision-free then
        Σ_t ← Compute covariance along trajectory
        cost = C_baseline(ξ) + k_m C_variance(Σ_t)
        if cost < mincost then
            mincost ← cost, ξ_min ← ξ
        end if
    end if
end for
return ξ_min
```

A. Variance Cost Functional

We augment the cost functional proposed in [24] with a cost associated with the visibility of each trajectory. For visibility, the autonomous vehicle is concerned not with its own estimate of position but rather the other vehicle's estimate of its position $\hat{\boldsymbol{x}}_{i,t}^j$. To capture the uncertainty of this estimate, we propose a cost associated with covariance of v_j's estimate, $\boldsymbol{\Sigma}_t = \mathbb{E}[\hat{\boldsymbol{x}}_{i,t}^{j2}]$. In contrast to other methods which indirectly minimize uncertainty (by minimizing time in blind spot or maximizing geometric field of view for the car), we explicitly model the covariance $\boldsymbol{\Sigma}_t$ and minimize the covariance cost through the trajectory. Importantly, since the covariance is a cumulative metric of uncertainty, we account for trajectories that enter and exit blind spots and consider the entire time-varying nature of uncertainty.

We propose two different cost metrics related to the estimate covariance, an average variance cost and terminal variance cost. In the first, we penalize the *average covariance*

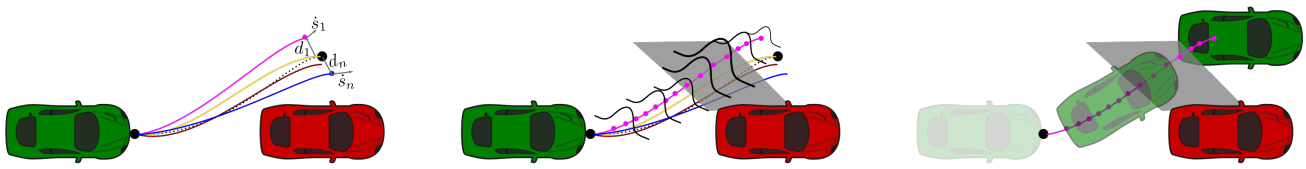

(a) Generate trajectories (b) Covariance computation and scoring (c) Trajectory selection

Fig. 3: Visibility-aware optimization. First, multiple trajectories are generated by specifying terminal conditions for quintic splines (Fig. 3a). The estimate covariance is calculated for each point along the trajectory (Fig. 3b), where position in blind spot leads to missed measurements by the leading vehicle (red). Trajectories are scored on a baseline comfort C_b and mean or terminal covariance cost C_m. The trajectory with lowest cost while remaining collision-free and dynamically feasible is returned to be executed by the vehicle (Fig. 3c).

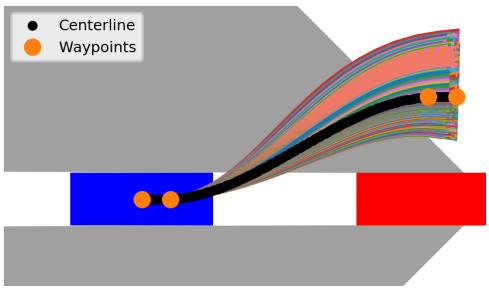

Fig. 4: Candidate trajectories generated during optimization. The centerline is specified by traffic maneuver waypoints.

over the entire trajectory

$$C_{mean}(\boldsymbol{\xi}) = C_{baseline}(\boldsymbol{\xi}) + k_m \sum_{t_j} \mathbb{E}[\hat{\boldsymbol{x}}^{j2}_{i,t_j}]. \tag{8}$$

In the second cost functional, only the *terminal covariance* is considered

$$C_{terminal}(\boldsymbol{\xi}) = C_{baseline}(\boldsymbol{\xi}) + k_m \mathbb{E}[\hat{\boldsymbol{x}}^{j2}_{i,T}]. \tag{9}$$

The benefit of considering only the terminal positional variance is that the terminal position may be the position of maximal interaction with the other vehicle, for example at the end of a lane change. On the other hand, during an overtaking maneuver when two vehicles interact at multiple points along the trajectory, an averaging approach is more appropriate. Additionally, by computing the covariance at each time step, thresholds can be added to the feasibility check during the initial generation of candidate trajectories (Fig. 4) to ensure that at no point does the covariance surpass a safety threshold.

The selection of weighting factor k_m determines the trade-off between a vehicle's own comfort and its visibility to other vehicles. As k_m increases, the trajectory generator biases towards trajectories that minimize time in blind spots. Having a variable weight allows users to choose the value of visibility (with respect to comfort) and level of desired proactiveness in planning. A safety conscious planner could choose a very high value for k_m whereas an aggressive driver may consider low values of k_m.

B. Modeling Blind Spot with Known Dynamics

The main type of occlusions that we consider is blind spots of other vehicles in traffic. Blind spots lead to asymmetric perception: the leading vehicle is unable to perceive the following ego vehicle while the ego vehicle can perceive the leading vehicle (and its blind spots). The asymmetry means that the leading vehicle will not sufficiently consider the ego vehicle's position in its motion planning, requiring that the ego vehicle take actions to improve its own visibility.

In the case where v_j knows v_i's dynamics, the system can be written as

$$\begin{aligned} \boldsymbol{x}_{i,t+1} &= f(\boldsymbol{x}_{i,t}, \boldsymbol{u}_{i,t}) + \boldsymbol{\omega}_t, & \boldsymbol{\omega}_t &\sim N(\boldsymbol{0}, \boldsymbol{Q}_t), \\ \boldsymbol{y}_t &= h(\boldsymbol{x}_{i,t}, \boldsymbol{u}_{i,t}) + \boldsymbol{\nu}_t, & \boldsymbol{\nu}_t &\sim N(\boldsymbol{0}, \boldsymbol{R}_t), \end{aligned} \tag{10}$$

where $\boldsymbol{\omega}_t$ and $\boldsymbol{\nu}_t$ are Gaussian process and measurement noises, respectively. We assume the system can be linearized about a known trajectory

$$\begin{aligned} \boldsymbol{x}_{i,t+1} &= \boldsymbol{A}_t \boldsymbol{x}_{i,t} + \boldsymbol{B}_t \boldsymbol{u}_{i,t} + \boldsymbol{\omega}_t, & \boldsymbol{\omega}_t &\sim N(\boldsymbol{0}, \boldsymbol{Q}_t), \\ \boldsymbol{y}_t &= \boldsymbol{C}_t \boldsymbol{x}_{i,t} + \boldsymbol{\nu}_t, & \boldsymbol{\nu}_t &\sim N(\boldsymbol{0}, \boldsymbol{R}_t), \end{aligned} \tag{11}$$

allowing v_j to use an EKF to estimate the position of the ego vehicle $\hat{\boldsymbol{x}}^j_{i,t}$

$$\hat{\boldsymbol{x}}^j_{i,t} = \boldsymbol{x}_{i,t} + \boldsymbol{L}_t(\boldsymbol{y}_t - \boldsymbol{C}_t \boldsymbol{x}_{i,t}). \tag{12}$$

This estimate can then be used by the leading vehicle v_j to plan safe trajectories without colliding with v_i.

The EKF gain and estimate covariance can be calculated as

$$\bar{\boldsymbol{\Sigma}}_t = \boldsymbol{A}_t \boldsymbol{\Sigma}_{t-1} \boldsymbol{A}_t^T + \boldsymbol{Q}_t, \tag{13}$$

$$\boldsymbol{S}_t = \boldsymbol{C}_t \boldsymbol{\Sigma}_t \boldsymbol{C}_t^T + \boldsymbol{R}_t, \tag{14}$$

$$\boldsymbol{L}_t = \bar{\boldsymbol{\Sigma}}_t \boldsymbol{C}_t^T \boldsymbol{S}_t^{-1}, \tag{15}$$

$$\boldsymbol{\Sigma}_t = \bar{\boldsymbol{\Sigma}}_t - \boldsymbol{L}_t \boldsymbol{C}_t \bar{\boldsymbol{\Sigma}}_t, \tag{16}$$

where $\bar{\boldsymbol{\Sigma}}_t$ is the a priori covariance, $\boldsymbol{S}_t$ the innovation, $\boldsymbol{L}_t$ the optimal Kalman gain and $\boldsymbol{\Sigma}_t$ the estimate covariance after assimilating measurement $\boldsymbol{y}_t$.

Blind spots are modeled as regions $\Xi_{blind} \in \mathbb{R}^2$ with high variance measurements, $\boldsymbol{R}_{t,blind} = \boldsymbol{\infty}$ whereas, when the vehicle is visible, measurements are received with covariance $\boldsymbol{R}_{t,seen}$. Effectively, v_j misses measurements and must propagate its estimates and corresponding variance from

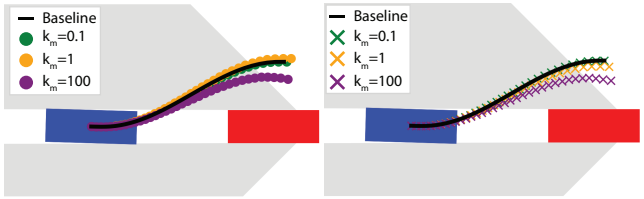

(a) Mean Covariance Cost (b) Terminal Covariance Cost

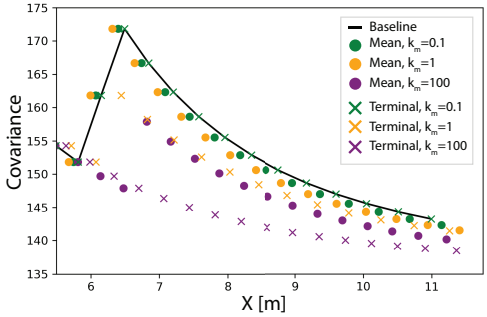

(c) Estimate Covariance Over Trajectory

Fig. 5: Visibility aware trajectories for a vehicle changing lanes while avoiding a stationary leading vehicle (red). For higher uncertainty score weights, the ego vehicle attempts to exit the blind spot earlier by either increasing velocity or deviating laterally from the baseline trajectory.

previous measurements. In addition, since both vehicles may be moving, the measurement covariance is computed as a function of both vehicles positions, $\boldsymbol{R}_t \sim R(\boldsymbol{x}_{i,t}, \boldsymbol{x}_{j,t})$ for each point along the trajectory.

C. Modeling Blind Spots with Unknown Dynamics

In scenarios where v_j does not have access to v_i's dynamics it is unlikely to formulate an estimate based on a Kalman filter. Instead, we consider a scenario where a range of control inputs is known by v_j. For example, in the case of an agent executing a braking trajectory, agent v_j may not know the dynamics of the car but can assume that the velocity is bounded $u_{\min} \leq |\dot{\boldsymbol{x}}_i| \leq u_{\max}$. The distribution of $\hat{\boldsymbol{x}}^j_{i,t}$ is then calculated by integrating the possible range of velocities over the duration of the trajectory. We assume that the variance is minimal before the blind spot $\mathbb{E}[\hat{\boldsymbol{x}}^{j2}_{i,t}] \approx 0 \, \forall t < t_{blind}$ where t_{blind} is the time that v_i enters the blind spot. In which case, $\hat{\boldsymbol{x}}^j_{i,t} \sim Uniform(T_{blind} u_{\min}, T_{blind} u_{\max})$ and the estimate covariance is

$$\mathbb{E}[\hat{\boldsymbol{x}}^{j2}_i] = \frac{1}{12} T^2_{blind} (u_{max} - u_{min})^2, \tag{17}$$

where $T_{blind} = T - t_{blind}$ is the time during which the agent is in the blind spot.

IV. Results

We simulate traffic scenarios for an ego vehicle v_i executing three different traffic maneuvers: changing lanes, entering an occluded intersection, and braking alongside a vehicle. In all scenarios, we consider both the baseline cost C_b and visibility cost C_m for each trajectory. The code utilizes the

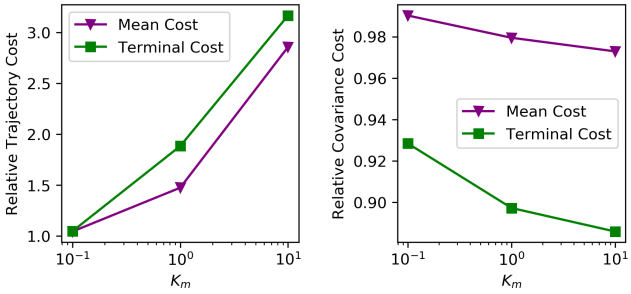

(a) Baseline Cost (b) Covariance Cost

Fig. 6: Mean cost relative to the baseline trajectory over 25 experiments. As the visibility weight k_m increases, trajectories are generated with reduced mean and terminal covariance costs as visibility is prioritized over the baseline cost (comfort and efficiency) of the trajectory.

the Python Robotics library [26] for initial implementation of [24] and polynomial spline solvers.

In all scenarios, the trajectory baseline cost is formulated as (5) with $k_{lat} = k_{lon} = 1$, $k_J = k_T = 0.1$ and $k_{\dot{s}} = 1.0$ ($k_s = 0$) and $k_s = 1.0$ ($k_{\dot{s}} = 0$) for speed following and position following, respectively. Unless otherwise specified, the following constraints are checked when generating trajectories: maximum speed $\dot{s} \leq 13$m/s, maximum acceleration $\ddot{s} \leq 2.0$m/s^2, and maximum trajectory curvature $\kappa \leq 11$/m.

A. Lane Change

In Fig. 5, the ego vehicle begins a lane change for overtaking a stopped green vehicle while minimizing a mean covariance cost (Fig. 5a) and terminal covariance cost (Fig. 5b). We randomly vary the initial and final position of the ego vehicle over 25 experiments. The ego vehicle begins with velocity $\dot{s}_0 = 2.77$ m/s and a final desired velocity of $\dot{s}^*_f = 8.33$m/s. The uncertainty of v_j's perception is modeled assuming linear dynamics (11) with $\boldsymbol{A}_t = \boldsymbol{0}$, $\boldsymbol{B}_t = \boldsymbol{I}$, $\boldsymbol{C}_t = \boldsymbol{I}$, and corresponding covariances $\boldsymbol{Q}_t = 10\boldsymbol{I}$, $\boldsymbol{R}_{seen,t} = 2000\boldsymbol{I}$, and $\boldsymbol{R}_{blind,t} = \boldsymbol{\infty}$. Combining the known dynamics with the EKF covariance (16) leads to an expression for the estimate covariance at each time step of the trajectory

$$\boldsymbol{\Sigma}_t = \frac{\boldsymbol{R}_t(\boldsymbol{\Sigma}_{t-1} + \boldsymbol{Q}_t)}{\boldsymbol{\Sigma}_{t-1} + \boldsymbol{Q}_t + \boldsymbol{R}_t}, \tag{18}$$

where $\boldsymbol{\Sigma}_{t-1}$ is the estimate covariance at the previous time step.

In Fig. 5c, the estimate covariance is plotted at each position along a relevant portion of the trajectory for one experiment. When the vehicle loses visibility ($x = 6$m) the covariance increases due to missed measurements. Higher visibility weights lead to lower variances over the entire trajectory. Figure 6 plots the mean baseline trajectory cost $C_{baseline}$ and covariance cost C_m relative to a baseline trajectory ($k_m = 0$) for 25 experiments. In Fig. 6a, as k_m increases, the baseline cost (jerk, lateral deviations, duration) increases to allow for increased visibility. Figure 6b shows the reduction in covariance cost for both the mean and

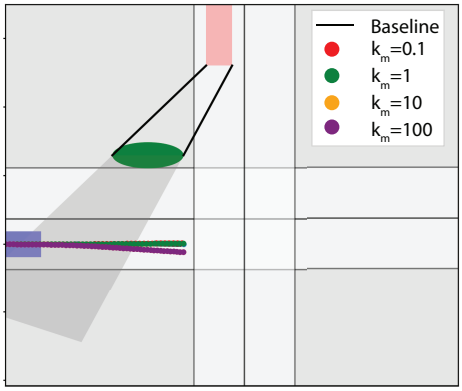

Fig. 7: Ego vehicle approaches an intersection with a visual obstruction along trajectory. Blind spots are calculated for a simulated cross-traffic vehicle (pink) occluded by shrubbery (green). Optimized trajectories for various visibility-aware weightings are plotted over the baseline trajectory.

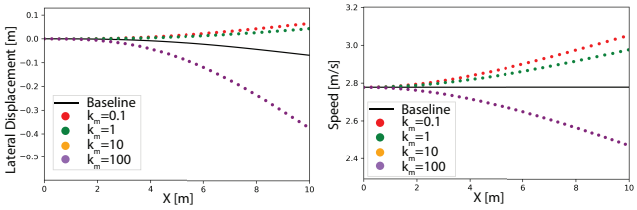

(a) Lateral Displacement (d) (b) Longitudinal Speed ($\dot{s}$)

Fig. 8: Displacements of trajectories in Frenet Frame for various visibility weights k_m in an occluded intersection scenario.

terminal covariance costs, with an improvement of over 10% when the optimization uses a terminal cost and $k_m = 10$.

B. Occluded Intersection

We also consider static obstacles such as shrubbery that may occlude part of the intersection as a vehicle approaches an intersection as shown in Fig. 7. The ego vehicle simulates a cross-traffic vehicle (pink) that enters at the same time as the ego vehicle. The ego vehicle attempts to minimize its lateral displacement while maintaining a final speed of $\dot{s}_f = \dot{s}_0 = 3.7$m/s. For lower values of k_m, the ego vehicle increases its speed to reduce time in the blind spot (Fig.8b) and for higher values, the ego vehicle departs laterally from the centerline to exit the occluded region earlier in its trajectory (Fig.8a).

C. Braking with Unknown Dynamics

In Fig. 9, an ego vehicle is braking before a vehicle while considering the visibility of a vehicle to its side. The specific dynamics of the ego vehicle are not known to the side vehicle but rather assumes that the ego vehicle's maximum speed is the speed at entering the blind spot ($\dot{\boldsymbol{x}}_{i,\max} = \dot{\boldsymbol{x}}_{i,t_{blind}}$) where t_{blind} is the time at which the ego vehicle loses visibility. The estimate covariance used for the visibility cost is calculated using (17) with $\boldsymbol{u}_{i,\min} = 0$

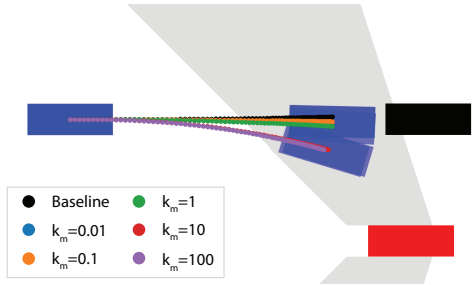

(a) Case 3: Braking Trajectories

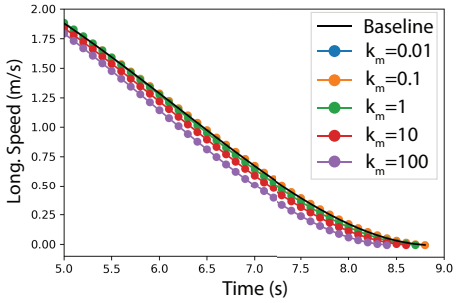

(b) Longitudinal Speed Profile

Fig. 9: In (a), the ego vehicle (blue) must brake to avoid colliding with a preceding vehicle (black). (b) Longitudinal speeds for the different weights, where slower speed profiles correspond to reduced uncertainty in position.

and $\boldsymbol{u}_{i,\max} = \dot{\boldsymbol{x}}_{i,t_{blind}}$ leading to variance cost

$$C_m = \mathbb{E}[\hat{\boldsymbol{x}}_{i,T}^{j2}] = \frac{1}{12}\dot{\boldsymbol{x}}_{t_{blind}}^2 (T - t_{blind})^2. \tag{19}$$

Figure 9a shows visibility-aware trajectories for various levels of visibility weighting k_m. Initial candidate trajectories are generated by sampling terminal conditions $[s_f, \dot{s}_f, \ddot{s}_f, T]_{ij}$ corresponding to the ego vehicle stopping before the vehicle in front with desired terminal speed $\dot{s}_f = \ddot{s}_f = 0$, terminal position $s_f \in [s_f^* - \Delta s, s_f^* + \Delta s]$ and $T_j \in [T^* - \Delta T, T^* + \Delta T]$ where s_f^* and T^* are desired braking distance and time, respectively. The quintics are checked for a maximum acceleration $\ddot{s}_{\max} = 4\text{m/s}^2$ and then scored using (19). Varying k_m leads to emergent behaviors of the ego vehicle such as lateral deviations from the centerline and slower longitudinal speed trajectories so as to decrease the possible future positions within the blind spot (Fig. 9b).

V. Conclusions

In this work, we consider optimizing trajectories of an ego vehicle to increase its visibility. Blind spots and obstacles are modeled as regions with missed measurements, leading to high variance estimates. By incorporating this variance into the trajectory cost, we can reduce the final estimate uncertainty by upwards of 10%. One limitation of the current approach is that we require an accurate model of the vehicles' motion for calculating the estimate uncertainty. Future work could consider incorporating the uncertainty of the leading vehicle's trajectory and future vehicle actions into the optimization.

REFERENCES

[1] X. Huang, S. G. McGill, B. C. Williams, L. Fletcher, and G. Rosman, "Uncertainty-Aware Driver Trajectory Prediction at Urban Intersections," in *2019 International Conference on Robotics and Automation (ICRA)*, May 2019, pp. 9718–9724.

[2] S. Primatesta, G. Guglieri, and A. Rizzo, "A Risk-Aware Path Planning Strategy for UAVs in Urban Environments," *Journal of Intelligent & Robotic Systems*, no. 95, pp. 629–643, 2019.

[3] J. Müller and G. S. Sukhatme, "Risk-aware trajectory generation with application to safe quadrotor landing," in *2014 IEEE/RSJ International Conference on Intelligent Robots and Systems*, Sep. 2014, pp. 3642–3648.

[4] W. Liu and M. H. Ang, "Incremental sampling-based algorithm for risk-aware planning under motion uncertainty," in *2014 IEEE International Conference on Robotics and Automation (ICRA)*, May 2014, pp. 2051–2058.

[5] S. Patil, J. van den Berg, and R. Alterovitz, "Estimating probability of collision for safe motion planning under Gaussian motion and sensing uncertainty," in *2012 IEEE International Conference on Robotics and Automation*, May 2012, pp. 3238–3244.

[6] Y. Ren, S. Elliott, Y. Wang, Y. Yang, and W. Zhang, "How Shall I Drive? Interaction Modeling and Motion Planning towards Empathetic and Socially-Graceful Driving," in *2019 International Conference on Robotics and Automation (ICRA)*, May 2019, pp. 4325–4331.

[7] Y. F. Chen, M. Everett, M. Liu, and J. P. How, "Socially aware motion planning with deep reinforcement learning," in *2017 IEEE/RSJ International Conference on Intelligent Robots and Systems (IROS)*, Sep. 2017, pp. 1343–1350.

[8] N. Buckman, A. Pierson, W. Schwarting, S. Karaman, and D. Rus, "Sharing is Caring: Socially-Compliant Autonomous Intersection Negotiation," in *IEEE/RSJ International Conference on Intelligent Robots and Systems (IROS)*, 2019.

[9] E. Pagello, A. D'Angelo, F. Montesello, F. Garelli, and C. Ferrari, "Cooperative behaviors in multi-robot systems through implicit communication," *Robotics and Autonomous Systems*, vol. 29, no. 1, pp. 65–77, 1999.

[10] C. Breazeal, C. D. Kidd, A. L. Thomaz, G. Hoffman, and M. Berlin, "Effects of nonverbal communication on efficiency and robustness in human-robot teamwork," in *2005 IEEE/RSJ International Conference on Intelligent Robots and Systems*, Aug 2005, pp. 708–713.

[11] D. Sadigh, S. S. Sastry, S. A. Seshia, and A. Dragan, "Information gathering actions over human internal state," in *2016 IEEE/RSJ International Conference on Intelligent Robots and Systems (IROS)*, Oct 2016, pp. 66–73.

[12] Y. Zhang, C. G. Cassandras, and A. A. Malikopoulos, "Optimal control of Connected Automated Vehicles at urban traffic intersections: A feasibility enforcement analysis," in *2017 American Control Conference (ACC)*, May 2017, pp. 3548–3553.

[13] A. Colombo and D. Del Vecchio, "Efficient Algorithms for Collision Avoidance at Intersections," in *Proceedings of the 15th ACM International Conference on Hybrid Systems: Computation and Control*, ser. HSCC '12. New York, NY, USA: ACM, 2012, pp. 145–154.

[14] D. Sadigh, S. Sastry, S. A. Seshia, and A. D. Dragan, "Planning for Autonomous Cars that Leverage Effects on Human Actions," in *Robotics: Science and Systems XII*. Robotics: Science and Systems Foundation, 2016.

[15] S. H. Huang, D. Held, P. Abbeel, and A. D. Dragan, "Enabling robots to communicate their objectives," *Autonomous Robots*, vol. 43, no. 2, pp. 309–326, 2019.

[16] M. Schwager, P. Dames, D. Rus, and V. Kumar, "A multi-robot control policy for information gathering in the presence of unknown hazards," in *Springer Tracts in Advanced Robotics*, vol. 100, 2017, pp. 455–472.

[17] G. L. Mariottini, S. Martini, and M. B. Egerstedt, "A switching active sensing strategy to maintain observability for vision-based formation control," *2009 IEEE International Conference on Robotics and Automation*, pp. 2637–2642, 2009.

[18] R. Platt, R. Tedrake, L. Kaelbling, and T. Lozano-Pérez, "Belief space planning assuming maximum likelihood observations," *Robotics: Science and Systems*, vol. 6, pp. 291–298, 2011.

[19] J. Van Den Berg, P. Abbeel, and K. Goldberg, "LQG-MP: Optimized path planning for robots with motion uncertainty and imperfect state information," *The International Journal of Robotics Research*, vol. 30, no. 7, pp. 895–913, 2011.

[20] A. Bry and N. Roy, "Rapidly-exploring random belief trees for motion planning under uncertainty," in *2011 IEEE International Conference on Robotics and Automation*, May 2011, pp. 723–730.

[21] D. Isele, R. Rahimi, A. Cosgun, K. Subramanian, and K. Fujimura, "Navigating occluded intersections with autonomous vehicles using deep reinforcement learning," in *2018 IEEE International Conference on Robotics and Automation (ICRA)*, May 2018, pp. 2034–2039.

[22] S. G. McGill, G. Rosman, T. Ort, A. Pierson, I. Gilitschenski, B. Araki, L. Fletcher, S. Karaman, D. Rus, and J. J. Leonard, "Probabilistic risk metrics for navigating occluded intersections," *IEEE Robotics and Automation Letters*, vol. 4, no. 4, pp. 4322–4329, Oct 2019.

[23] H. Andersen, W. Schwarting, F. Naser, Y. H. Eng, M. H. Ang, D. Rus, and J. Alonso-Mora, "Trajectory optimization for autonomous overtaking with visibility maximization," in *2017 IEEE 20th International Conference on Intelligent Transportation Systems (ITSC)*, Oct 2017, pp. 1–8.

[24] M. Werling, J. Ziegler, S. Kammel, and S. Thrun, "Optimal trajectory generation for dynamic street scenarios in a Frenét Frame," in *2010 IEEE International Conference on Robotics and Automation*, May 2010, pp. 987–993.

[25] A. Takahashi, T. Hongo, Y. Ninomiya, and G. Sugimoto, "Local Path Planning And Motion Control For Agv In Positioning," in *Proceedings. IEEE/RSJ International Workshop on Intelligent Robots and Systems (IROS '89) 'The Autonomous Mobile Robots and Its Applications'*, Sep. 1989, pp. 392–397.

[26] A. Sakai, D. Ingram, J. Dinius, K. Chawla, A. Raffin, and A. Paques, "PythonRobotics: a Python code collection of robotics algorithms," https://github.com/AtsushiSakai/PythonRobotics, 2018.